Supporting Information

Influence of Rb/Cs cation-exchange on inorganic Sn halide perovskites: From chemical structure to physical properties

Young-Kwang Jung,[†,¶] Ji-Hwan Lee,[†,¶] Aron Walsh,[*,†,‡] and Aloysius Soon[*,†]

†*Global E^3 Institute and Department of Materials Science and Engineering, Yonsei University, Seoul, South Korea*

‡*Department of Materials, Imperial College London, London, United Kingdom*

¶*Contributed equally to this work.*

E-mail: a.walsh@imperial.ac.uk; aloysius.soon@yonsei.ac.kr

Bulk properties

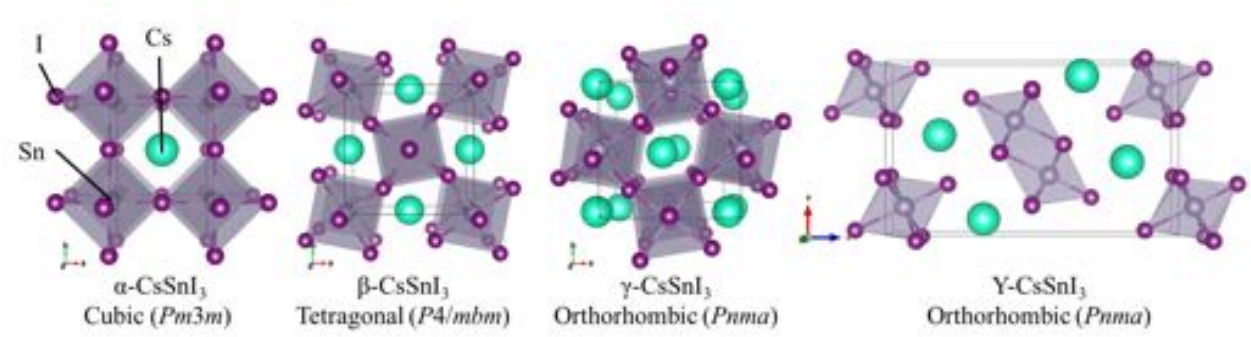

Figure S1: Atomic structure of $CsSnI_3$ polymorphs.

In this study, we have tested the influence of spin-orbit coupling (SOC) effect on the structural optimization of $CsSnI_3$, using the γ phase as an example. Our PBE+SOC results show very small (i.e. negligible) changes of less than 0.01 Å for the lattice constants, less than 0.01 ° for the Sn–I–Sn bonding angles, and less than 0.01 eV for the band gap. Therefore, we argue that the use of PBE (without SOC) for structural optimization is adequate for this study.

Table S1: Bulk properties of polymorphs of $CsSnI_3$ and $RbSnI_3$. Lattice constants of unit cells (a_0, b_0, and c_0) are in unit of Å, average tilting angles ($\bar{\theta}_{ab}$ and $\bar{\theta}_c$) are in unit of degree (°), standard formation enthalpy of polymorphs (ΔH_f) is in unit of eV/formula unit, and bulk modulus (B_0) is in the unit of GPa, respectively.

	a_0	b_0	c_0	$\bar{\theta}_{ab}$	$\bar{\theta}_c$	ΔH_f	B_0
α-$CsSnI_3$	6.28[a]	6.28[a]	6.28[a]	0.00[a]	0.00[a]	-4.77[a]	15.35[a]
	6.29[b]	6.29[b]	6.29[b]	–	–	–	18.33[c]
	6.21[d]	6.21[d]	6.21[d]	–	–	–	–
β-$CsSnI_3$	8.77[a]	8.77[a]	6.35[a]	22.49[a]	0.00[a]	-4.80[a]	14.58[a]
	8.77[b]	8.77[b]	6.36[b]	–	–	–	17.45[c]
	8.72[d]	8.72[d]	6.19[d]	–	–	–	–
γ-$CsSnI_3$	8.94[a]	8.69[a]	12.52[a]	23.98[a]	19.14[a]	-4.82[a]	9.75[a]
	8.94[b]	8.71[b]	12.50[b]	–	–	–	15.92[c]
	8.69[d]	8.64[d]	12.38[d]	–	–	–	–
Y-$CsSnI_3$	10.82[a]	4.82[a]	18.12[a]	–	–	-4.82[a]	–
	10.28[c]	4.73[c]	17.57[c]	–	–	–	13.07[c]
	10.35[d]	4.76[d]	17.68[d]	–	–	–	–
α-$RbSnI_3$	6.25[a]	6.25[a]	6.25[a]	0.00[a]	0.00[a]	-4.47[a]	15.37[a]
β-$RbSnI_3$	8.65[a]	8.65[a]	6.32[a]	30.45[a]	0.00[a]	-4.58[a]	15.04[a]
γ-$RbSnI_3$	8.93[a]	8.47[a]	12.28[a]	31.98[a]	30.42[a]	-4.64[a]	10.24[a]
Y-$RbSnI_3$	10.74[a]	4.78[a]	17.51[a]	–	–	-4.65[a]	–

[a] This work
[b] Theoretical values from Ref. 1
[c] Theoretical values from Ref. 2
[d] Experimental values from Ref. 3

Table S2: Electronic band gap of γ-$CsSnI_3$ and $RbSnI_3$ for different exchange correlation functionals (xc). For semi-local xc (PBE), we used a **k**-points grids of $6 \times 6 \times 5$ with and without spin-orbit coupling (xc and xc+SOC). For hybrid functionals (HSE06), we used a less dense **k**-points grids of $3 \times 3 \times 3$ and various cut-off energy (E_{cut}). The cut-off energy of 300 eV hardly affects to the value of E_{g} in HSE06 with comparison to E_{g} with 600 eV of E_{cut}. Also the SOC effects on E_{g} (ΔE_{g} which is defined as $E_{\mathrm{g}}[xc + \mathrm{SOC}] - E_{\mathrm{g}}[xc]$) show a similarity for different xc of PBE and HSE06.

	xc	E_{cut} (eV)	**k**-point	$E_{\mathrm{g}}[xc]$	$E_{\mathrm{g}}[xc$+SOC]	ΔE_g
γ-$CsSnI_3$	PBE[a]	600	$6 \times 6 \times 5$	0.824	0.491	0.333
	HSE06[a]	600	$3 \times 3 \times 3$	1.213		
	HSE06[a]	300	$3 \times 3 \times 3$	1.213	0.858	0.356
	PBE[b]	300	$1 \times 1 \times 2$		0.52	
	HSE[c]	500	$4 \times 4 \times 4$		1.19	
	QSGW[d]				1.37	
	GW_0[e]	500			1.34	
γ-$RbSnI_3$	PBE[a]	600	$6 \times 6 \times 5$	0.992	0.727	0.264
	HSE06[a]	600	$3 \times 3 \times 3$	1.409		
	HSE06[a]	300	$3 \times 3 \times 3$	1.409	1.128	0.282
	HSE[c]	500	$4 \times 4 \times 4$		1.72	

[a] This work
[b] From Ref. 4, GGA-PBE and **k**-points are supercell including 80 atoms
[c] From Ref. 5, HSE with including 65 % of exact exchange
[d] From Ref. 4, Quasiparticle self-consistent GW calculation (QSGW)
[e] From Ref. 6, GW_0 calculation with using converged **k**-points grid

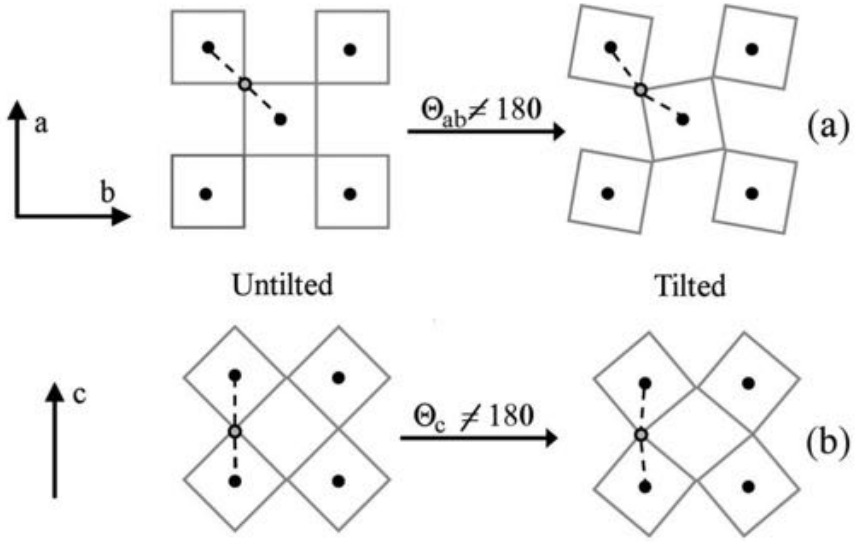

(a) Schematic definition of distortion angles (Θ_{ab} and Θ_c) in perovskite.

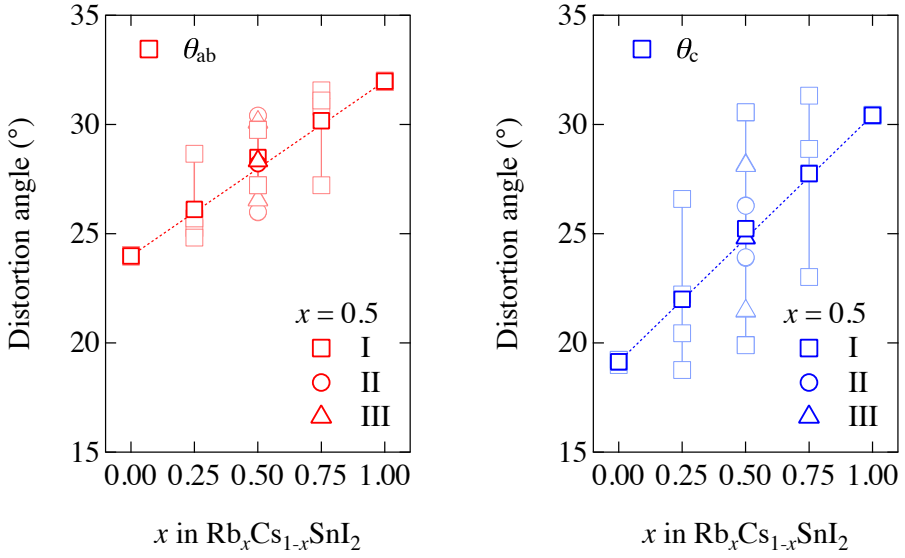

(b) The distortion angles as function of x in $Rb_xCs_{1-x}SnI_3$.

Figure S2: Detailed information for distortion angles in bulk. (a) Θ_{ab} is defined as an angle between Sn-I-Sn bridge within ab-plane and Θ_c is defined as angle of I-Sn-I bridge along c-axis. This figure is adapted from Figure 2 of Ref. 7. Here we define distortion angle θ, where $\theta = 180\,^\circ - \Theta$. (b) The blue and red markers are average values of the light blue and light red markers at each x in $Rb_xCs_{1-x}SnI_3$, respectively.

Table S3: Ground state properties of x in γ-$Rb_xCs_{1-x}SnI_3$, such as lattice parameters (a_0, b_0, and c_0 in unit of Å), average tilting angles ($\bar{\theta}_{ab}$ and $\bar{\theta}_c$ in unit of °), and band gap without and with SOC (E_g^{PBE} and $E_g^{PBE+SOC}$ in unit of eV) of $Rb_xCs_{1-x}SnI_3$. The influence of SOC on band gap are calculated as ΔE_g in unit of eV, which is defined as $E_g^{PBE+SOC} - E_g^{PBE}$. The internal energy ($\Delta U$) and entropy ($\Delta S$) of mixing are in unit of eV/cation and meV/cation·K, respectively.

x	a_0	b_0	c_0	$\bar{\theta}_{ab}$	$\bar{\theta}_c$	E_g^{PBE}	$E_g^{PBE+SOC}$	ΔE_g	ΔU	ΔS
0.00	8.94	8.69	12.52	23.98	19.14	0.82	0.49	0.33	0.0000	0.0000
0.25	8.95	8.64	12.47	28.49	25.23	0.88	0.57	0.31	0.0066	0.0485
0.50-I	9.00	8.56	12.40	26.11	22.00	0.98	0.69	0.29	0.0092	0.0597
0.50-II	8.94	8.59	12.41	28.20	25.10	0.91	0.62	0.29	0.0107	0.0597
0.50-III	8.95	8.57	12.41	28.33	24.80	0.93	0.64	0.29	0.0093	0.0597
0.75	8.94	8.53	12.35	30.17	27.75	0.97	0.70	0.27	0.0097	0.0485
1.00	8.93	8.47	12.28	31.98	30.42	0.99	0.73	0.26	0.0000	0.0000

Surface properties

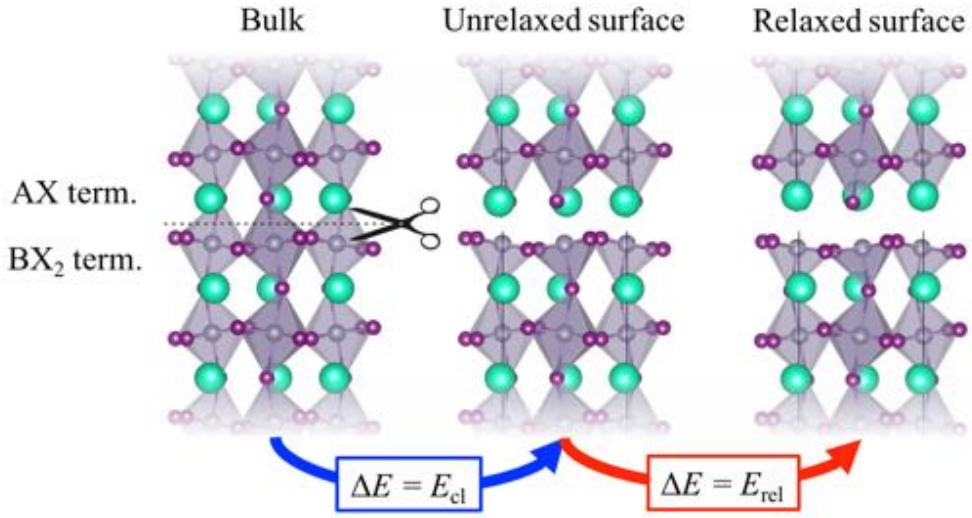

Figure S3: Schematic flow of surface energy calculation from bond cleaving (E_{cl}) and surface relaxation (E_{rel}) approach.

In order to compare the relative energetic stability of two different terminations (AX or BX_2 terminations) of $ABX_3(001)$ perovskite surface, which are not stoichiometric, we calculate surface energies based on bond cleaving and surface relaxation approach from Refs. 8,9. Within this approach, the surface energy is defined as a summation of the cleaving energy (E_{cl}) and relaxation energy (E_{rel}). Here, E_{cl} is assumed to be distributed equally between created surfaces due to the fact that two different terminations of $ABX_3(001)$ occur simultaneously during cutting the bulk into two slabs. Therefore, the surface energy with a termination t ($E_{\mathrm{surf}}(t)$, where t = AX or BX_2) is represented as,

$$E_{\mathrm{surf}}(t) = E_{\mathrm{cl}} + E_{\mathrm{rel}}(t) \quad . \tag{1}$$

E_{cl} is obtained via the following

$$E_{\mathrm{cl}} = \frac{1}{4A}\left[E_{\mathrm{slab}}^{\mathrm{unrel}}(t_1) + E_{\mathrm{slab}}^{\mathrm{unrel}}(t_2) - \frac{N_{\mathrm{slab}}^{\mathrm{atom}}(t_1) + N_{\mathrm{slab}}^{\mathrm{atom}}(t_2)}{N_{\mathrm{bulk}}^{\mathrm{atom}}} E_{\mathrm{bulk}}\right] \quad . \tag{2}$$

Here, the factor 1/4 is attributed to the fact that totally four exposed surfaces are taken

Table S4: The cleaving energy (E_{cl}), relaxation energy (E_{rel}) and the surface energy ($E_{\mathrm{surf}} = E_{\mathrm{cl}} + E_{\mathrm{rel}}$) of $RbSnI_3(001)$ with RbI and SnI_2 termination, and $CsSnI_3(001)$ with CsI and SnI_2

($meV/Å^2$)	E_{cl}	E_{rel}	E_{surf}
$CsSnI_3(001)$:CsI	8.03	-2.31	5.73
$CsSnI_3(001)$:SnI_2	8.03	-1.98	6.05
$RbSnI_3(001)$:RbI	8.42	-3.18	5.24
$RbSnI_3(001)$:SnI_2	8.42	-2.33	6.09

into account. $E^{\mathrm{unrel}}_{\mathrm{slab}}(t_1)$, $E^{\mathrm{unrel}}_{\mathrm{slab}}(t_2)$, and E_{bulk} are total energy of unrelaxed t_1 terminated slab, unrelaxed t_2 terminated slab, and bulk, respectively. $N^{\mathrm{atom}}_{\mathrm{slab}}(t_1)$, $N^{\mathrm{atom}}_{\mathrm{slab}}(t_2)$, and $N^{\mathrm{atom}}_{\mathrm{bulk}}$ are the total number of atoms in each atomic models of t_1 terminated slab, t_2 terminated slab, and bulk respectively. For example, if $CsSnI_3(001)$:CsI, $CsSnI_3(001)$:SnI_2 slabs and bulk orthorhombic $CsSnI_3$ contain 54, 56, and 20 atoms ($N^{\mathrm{atom}}_{\mathrm{slab}}$(CsI) and $N^{\mathrm{atom}}_{\mathrm{slab}}$($SnI_2$) and $N^{\mathrm{atom}}_{\mathrm{bulk}}$ are 54, 56, and 20 respectively), 5.5 would be used as a coefficient of E_{bulk}. The calculated E_{cl} is defined as the same for both terminations. $E_{\mathrm{rel}}(t)$ is obtained via the following

$$E_{\mathrm{rel}}(t) = \frac{1}{2A}\left[E^{\mathrm{rel}}_{\mathrm{slab}}(t) - E^{\mathrm{unrel}}_{\mathrm{slab}}(t)\right] \tag{3}$$

where $E^{\mathrm{rel}}_{\mathrm{slab}}(t)$ and $E^{\mathrm{unrel}}_{\mathrm{slab}}(t)$ are total energies of relaxed and unrelaxed slab with t termination. Here, A denotes the surface area of the slab model. The factor 1/2 is considered because there are two exposed surfaces in the slab models. The calculated E_{cl}, E_{rel}, and E_{surf} are tabulated in Table S4 and comparison with *ab initio* atomistic thermodynamics (*ai*AT) are shown in Figure S4.

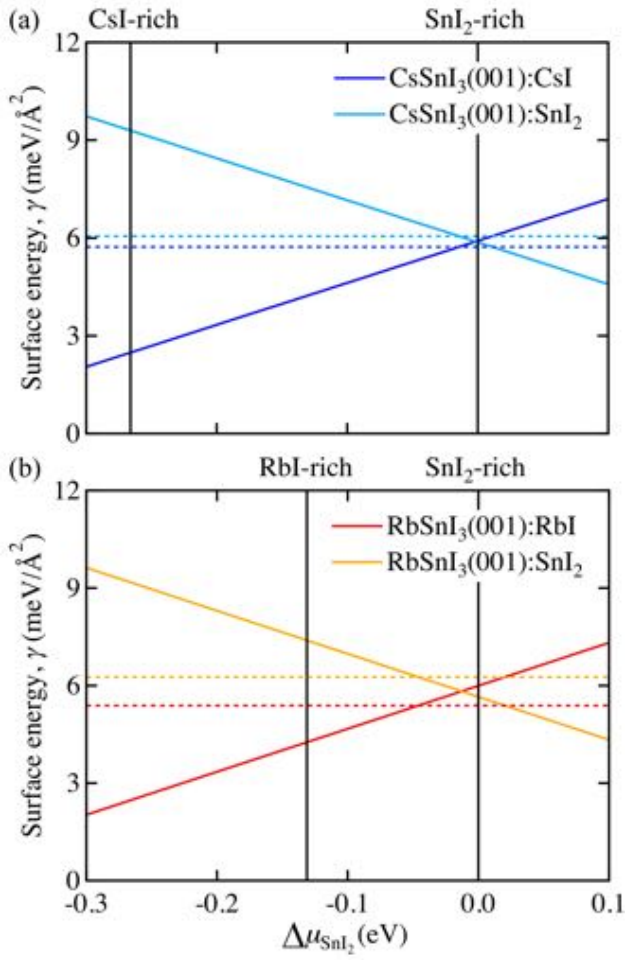

Figure S4: Comparison between *ai*AT approach and bond cleaving and surface relaxation approach in calculating surface energy. Solid lines stand for surface energy from *ai*AT approach and dashed lines stand for surface energy from bond cleaving and surface relaxation approach. Although bond cleaving and surface relaxation approach cannot show environmental dependency of surface energy like *ai*AT approach, it produces comparable order of surface energy values with *ai*AT.

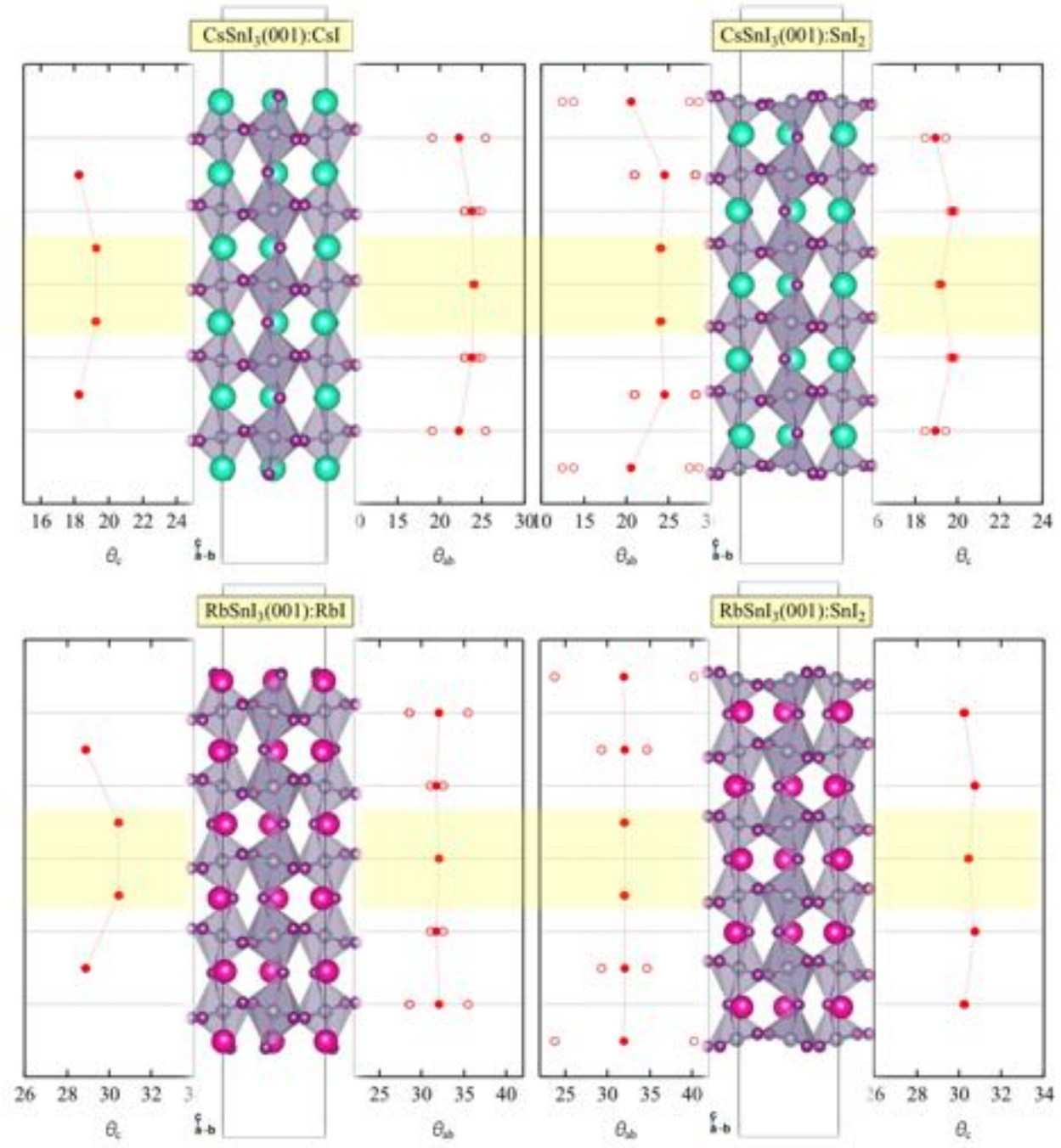

Figure S5: Detailed information for distortion angles in slab. The yellow box regions are bulk-like region by not allowing relaxation. The red dots are average values at each layer.

Table S5: The absolute band edge levels with respect to the vacuum level (E_{VBM} and E_{CBM}) are calculated in unit of eV for slabs with different terminations of $CsSnI_3$ and $RbSnI_3$. The semi-local exchange-correlation (xc) functional of PBE and hybrid functional of HSE06 with and without SOC are considered. The influence of SOC are calculated as ΔE which is defined as $E^{xc+\mathrm{SOC}} - E^{xc}$.

xc	$CsSnI_3$(001):CsI		$CsSnI_3$(001):SnI_2		$RbSnI_3$(001):RbI		$RbSnI_3$(001):SnI_2	
	E_{CBM}	E_{VBM}	E_{CBM}	E_{VBM}	E_{CBM}	E_{VBM}	E_{CBM}	E_{VBM}
PBE	−2.87	−3.70	−4.53	−5.35	−3.00	−3.99	−4.43	−5.43
PBE+SOC	−3.17	−3.66	−4.82	−5.31	−3.23	−3.95	−4.66	−5.39
ΔE	−0.30	0.04	−0.29	0.04	−0.23	0.04	−0.23	0.04
HSE06	−2.72	−4.93	−4.44	−5.65	−3.85	−4.26	−4.33	−5.74
HSE06+SOC	−3.03	−3.89	−4.75	−5.60	−3.08	−4.21	−4.57	−5.70
ΔE	−0.31	0.04	−0.31	0.05	−0.23	0.05	−0.24	0.04

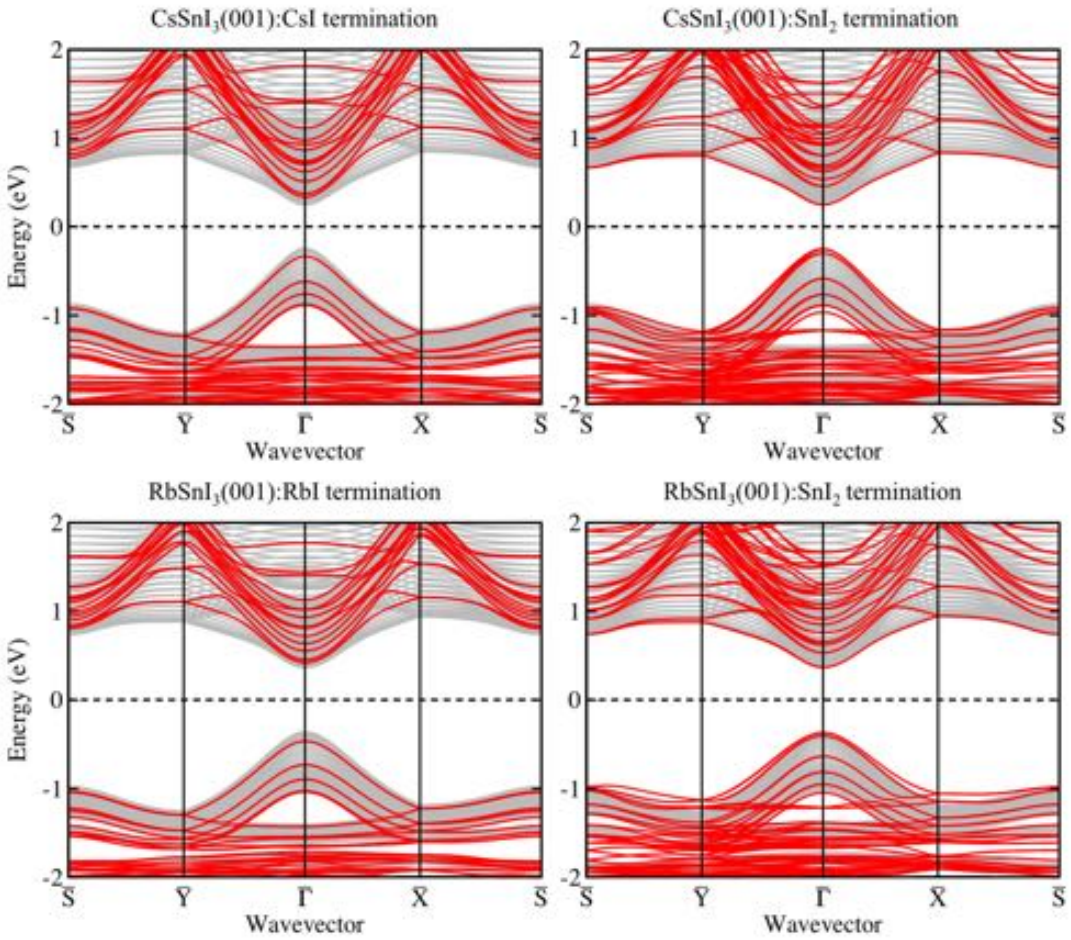

Figure S6: Surface band structures of $CsSnI_3$ and $RbSnI_3$ (001) slab models from PBE+SOC where slab structures are same with Figure 4 in main text. The shaded (gray) lines and red lines correspond to the bulk and slab bands. The Fermi level is set to 0 eV. Calculated band gaps 0.67 eV, 0.50 eV, 0.88 eV, and 0.74 eV for $CsSnI_3$(001):CsI, $CsSnI_3$(001):SnI_2, $RbSnI_3$(001):RbI, and $RbSnI_3$(001):SnI_2 slabs, respectively. $CsSnI_3$(001):CsI and $RbSnI_3$(001):RbI slabs show increased band gaps with respect to their bulk band gaps, while SnI_2 terminated slabs show almost same band gaps with respect to their bulk band gaps.

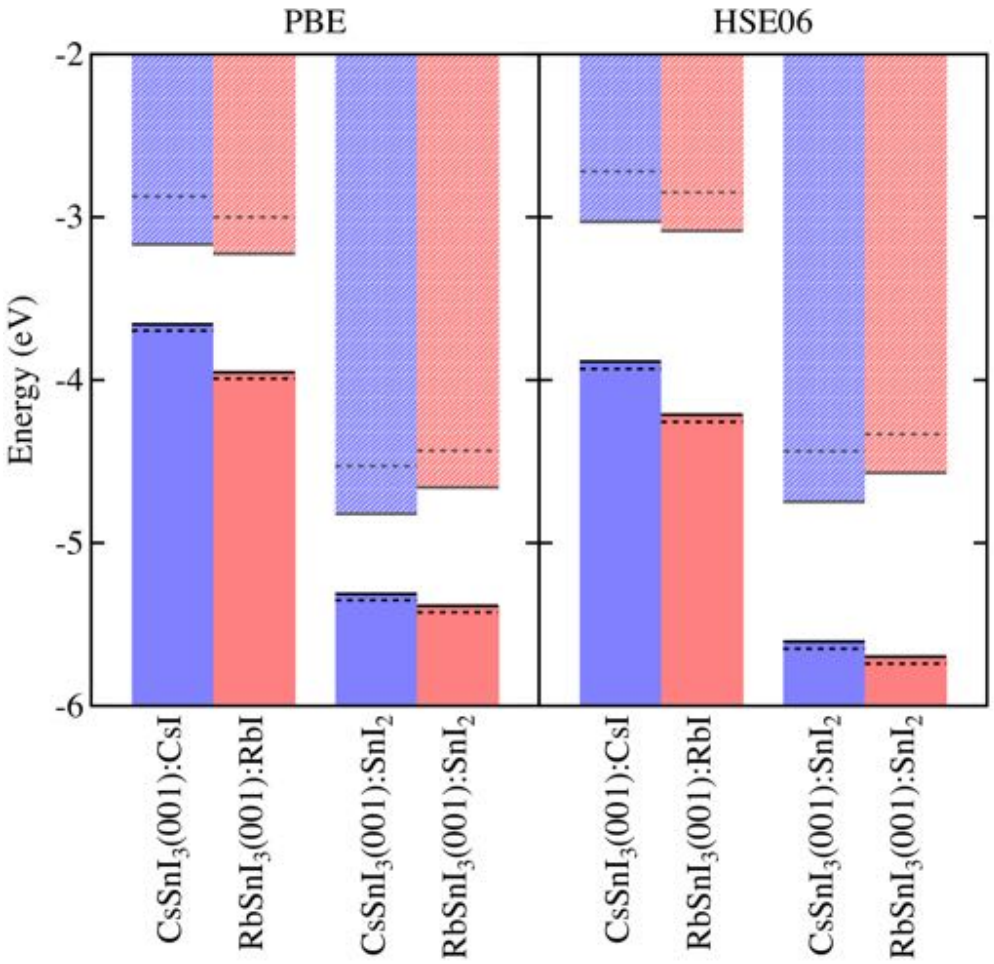

Figure S7: Band alignment of $CsSnI_3$ and $RbSnI_3$ with respect to the vacuum level. The solid lines and dotted lines represent band levels with and without SOC effect. The HSE06 widen the band gap for both $CsSnI_3$ and $RbSnI_3$.

References

(1) Grote, C.; Berger, R. F. Strain Tuning of Tin-Halide and Lead-Halide Perovskites: A First-Principles Atomic and Electronic Structure Study. *J. Phys. Chem. C* **2015**, *119*, 22832.

(2) da Silva, E. L.; Skelton, J. M.; Parker, S. C.; Walsh, A. Phase stability and transformations in the halide perovskite $CsSnI_3$. *Phys. Rev. B* **2015**, *91*, 144107.

(3) Chung, I.; Song, J.-H.; Im, J.; Androulakis, J.; Malliakas, C. D.; Li, H.; Freeman, A. J.; Kenney, J. T.; Kanatzidis, M. G. $CsSnI_3$: Semiconductor or Metal? High Electrical Conductivity and Strong Near-Infrared Photoluminescence from a Single Material. High Hole Mobility and Phase-Transitions. *J. Am. Chem. Soc.* **2012**, *134*, 8579.

(4) Xu, P.; Chen, S.; Xiang, H.-J.; Wei, S.-H.; Gong, X.-G. Influence of Defects and Synthesis Conditions on the Photovoltaic Performance of Perovskite Semiconductor $CsSnI_3$. *Chem. Mater.* **2014**, *26*, 6068–6072.

(5) Gou, G.; Young, J.; Liu, X.; Rondinelli, J. M. Interplay of Cation Ordering and Ferroelectricity in Perovskite Tin Iodides: Designing a Polar Halide Perovskite for Photovoltaic Applications. *Inorg. Chem.* **2017**, *56*, 26–32.

(6) Lang, L.; Zhang, Y.-Y.; Xu, P.; Chen, S.; Xiang, H. J.; Gong, X. G. Three-Step Approach for Computing Band Offsets and Its Application to Inorganic ABX_3 Halide Perovskites. *Phys. Rev. B* **2015**, *92*, 075102.

(7) Borriello, I.; Cantele, G.; Ninno, D. Ab initio Investigation of Hybrid Organic-Inorganic Perovskites Based on Tin Halides. *Phys. Rev. B* **2008**, *77*, 235214.

(8) Heifets, E.; Eglitis, R. I.; Kotomin, E. A.; Maier, J.; Borstel, G. Ab Initio Modeling of Surface Structure for $SrTiO_3$ Perovskite Crystals. *Phys. Rev. B* **2001**, *64*, 235417.

(9) Eglitis, R. I. Ab Initio Hybrid DFT Calculations of $BaTiO_3$, $PbTiO_3$, $SrZrO_3$ and $PbZrO_3$ (111) Surfaces. *Appl. Surf. Sci.* **2015**, *358*, 556–562.